Biosensors and Bioelectronics 290 (2025) 118002

Contents lists available at ScienceDirect

Biosensors and Bioelectronics

journal homepage: www.elsevier.com/locate/bios

Imidazole-enhanced luminol/H_2O_2 chemiluminescent biosensing for SARS-CoV-2 nucleocapsid protein with enzymatic regulation of hemin switch☆

Hang Ao [a,b], Jinshan Xiong [b], Wencheng Xiao [a], Wenrui Hu [a], Jie Wu [a,*], Huangxian Ju [a,**]

[a] State Key Laboratory of Analytical Chemistry for Life Science, School of Chemistry and Chemical Engineering, Nanjing University, Nanjing, 210023, PR China
[b] School of Chemistry and Materials Science, Guizhou Normal University, Guiyang, 550025, PR China

ARTICLE INFO

Keywords:
Chemiluminescence imaging
Immunoassay
DNA nanomachine
Proximity assembly
SARS-CoV-2 nucleocapsid protein
DNAzyme

ABSTRACT

Owing to the continuous mutations of the coronavirus, the sensitive and accurate detection of the SARS-CoV-2 nucleocapsid protein is still necessary in clinical diagnosis. Aim to the challenge of sensitivity in chemiluminescence (CL) imaging detection and the need for high-throughput clinical screening, this work used imidazole (Im) as an enhancer for hemin-DNA/luminol/H_2O_2 CL system to propose a CL imaging method for SARS-CoV-2 nucleocapsid protein detection. In this system Im could reduce the hemin-DNA catalyzed oxidation energy of luminol by H_2O_2 to promote the CL emission through the accelerated breaking of O-O bond of dianionic cyclic peroxide. The enhancement mechanism was demonstrated with theoretical calculations and several characterization techniques. By combining the proximity-induced initiator release with immunological recognition, an initiator-triggered DNA nanomachine was designed to achieve the release of abundant primers for activating hemin-DNA switch. This signal amplification strategy led to strong CL emission for highly sensitive imaging detection of the target. The Im-enhanced hemin-DNA/luminol/H_2O_2 CL imaging assay exhibited a linear detection range over 4 orders of magnitude with a detection limit down to 2.75 pg/mL for SARS-CoV-2 nucleocapsid protein, exhibiting promising potential of both Im sensitization and the proposed DNA nanomachine to improve the sensitivity of high-throughput CL biosensing for the early diagnosis and clinical screening of the coronavirus and other diseases.

1. Introduction

The severe acute respiratory syndrome coronavirus 2 (SARS-CoV-2) has been widely spread and its duration has been prolonged since 2019. Therefore, the controlling and reducing of the virus's transmission remains a challenge due to the rapid mutation of SARS-CoV-2 (Davis et al., 2023), and the detection of this virus remains crucial for early diagnosis of the disease and control of the epidemic. Although the real-time polymerase chain reaction provides the gold standard test for the virus gene, the requires of skilled operator, specialized laboratories and expensive equipment limit its application in underdeveloped areas (Diao et al., 2021; Shan et al., 2021). The immunoassay of SARS-CoV-2-related proteins provides a less expensive and easier way for the early pathogenic diagnose, and the serological analysis also improves the accurate diagnostic methods and helps epidemiologic studies (Anderson et al., 2021; Kim et al., 2022). Among the four structural proteins of SARS-CoV-2, including spike protein, envelope protein, membrane protein and nucleocapsid protein (NP), the SARS-CoV-2 NP has a low frequency of mutations and high expression level in human blood (Li et al., 2020; Ogata et al., 2020), which has been used as a priority diagnostic biomarker for the early diagnosis.

Commonly used protein assays for SARS-CoV-2 NP in clinical practice nowadays include the general enzyme-linked immunosorbent assay (ELISA) (Wang et al., 2023; L. Guo et al., 2020; Ferreira et al., 2023), lateral flow immunoassay (LFIA) (Perveen et al., 2023; Kilic et al., 2020; Sun et al., 2022) and chemiluminescence immunoassay (CLIA) (Zhang et al., 2021; Lyu et al., 2021; Xu et al., 2022). The ELISA provides reliable detection results for protein target, but suffers from the multiple

☆ Published in honor of the 90th birthday of Professor Ruqin Yu.

* Corresponding author.
** Corresponding author.
E-mail addresses: wujie@nju.edu.cn (J. Wu), hxju@nju.edu.cn (H. Ju).

https://doi.org/10.1016/j.bios.2025.118002
Received 18 June 2025; Received in revised form 9 August 2025; Accepted 19 August 2025
Available online 16 September 2025

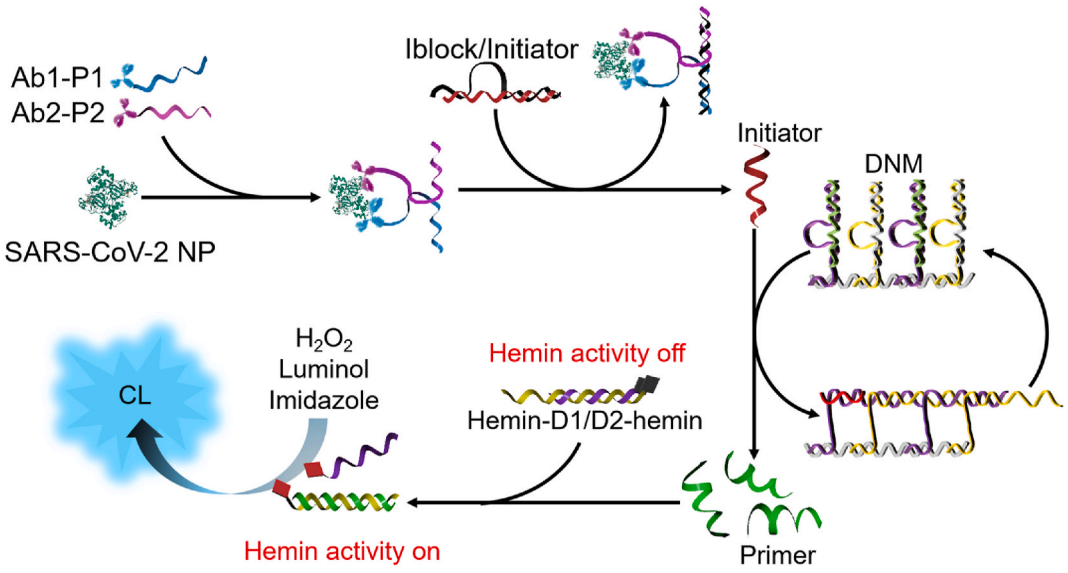

Scheme 1. Schematic illustration of CL imaging assay of SARS-CoV-2 NP with proximity-activated DNA nanomachine (DNM) to induce hemin-DNA activity regulation.

time-consuming washing and incubation steps. LFIA achieves rapid detection of proteins, but it also has drawbacks of low sensitivity and poor qualitative ability. CLIA is gradually becoming the mainstream detection protocol for protein biomarkers due to the high sensitivity and cost-effectiveness of CL assays (Xiao and Xu, 2020; Shi et al., 2023; Shi et al., 2025). Especially, the homogeneous CLIA has advantages of simple operation process, short assay time, low-cost devices and direct detection of analytes with high sensitivity and wide detection range, which make it more popular in clinical analyses (Takkinen and Žvirblienė, 2019; Rani et al., 2023). Besides, CL signals can be captured in a large imaging area by a charge coupled device, which benefits the high-throughput analysis based on CL imaging detection and enables the point-of-care testing through the portable devices such as smartphone (Liu et al., 2021; Lai et al., 2019).

Homogeneous CLIA for protein biomarkers using G-quadruplex/hemin has been developed (Zhang et al., 2021; Ao et al., 2023), but its flexibility is limited due to the inherent instability of hemin and the specific requirement of G4 sequences (Golnak et al., 2015; Alsharabasy et al., 2021). The hemin activity regulation method based on DNA-grafted hemin (hemin-DNA) provides a promising prospect for the construction of homogeneous CLIA. The activity regulation of hemin moiety can be achieved by DNA hybridization to separate hemin dimer at the ends of double strands into monomers, which recovers the activity of hemin (Wang et al., 2014, 2015). This DNA hybridization-induced activity regulation strategy for heme-DNA has been successfully applied in fluorescence (FL) assays and colorimetric assays, but the application of this strategy in chemiluminescence imaging assays is limited because of the relatively low catalytic activity of hemin moiety in luminol-based CL systems. Therefore, the development of hemin-DNA catalyzed luminol-based CL systems for the construction of homogeneous CLIA is still necessary. In this work, an imidazole (Im) enhanced hemin-DNA/luminol/H_2O_2 CL system was proposed for CL imaging detection of SARS-CoV-2 NP through a proximity-activated DNA nanomachine (DNM) to induce hemin-DNA activity regulation (Scheme 1). After the target was recognized by a pair of affinity probes, this signal amplification strategy and Im-enhanced CL emission led to strong CL emission for highly sensitive imaging detection of the SARS-CoV-2 NP. The proposed CL assay achieved rapid and sensitive detection of SARS-CoV-2 NP with a detection limit of 2.75 pg/mL, exhibiting a promising prospect for the early diagnosis of SARS-CoV-2-related diseases.

2. Experimental

2.1. Materials and reagents

Luminol, *p*-iodophenol, naphthol, L-histidine, L-arginine, polyvinyl pyrrolidone, L-lysine homopolymer hydrobromide, chitosan, 1,2,4-triazole (Tz), pyrazole (Pz), DMSO-*d*6, K_2HPO_4, KH_2PO_4, tris(2-carboxyethyl) phosphine hydrochloride (TCEP) and 3-maleimidobenzoic N-hydroxysuccinimide ester (MBS) were purchased from Sigma-Aldrich Co. (Shanghai, China). Imidazole (Im), 2-methylimidazole and imidazole-2-carboxaldehyde were bought from Aladdin Biochemical Technology Co., Ltd. (Shanghai, China). 4-Chlorothiophenol, 1,4-naphthalenedicarboxylic acid and tryptophan were purchased from InnoChem Science Technology Co. Ltd (Beijing, China). 1H-benzotriazole (BZTA) was bought from Meryer Biochemical Technology Co., Ltd. (Shanghai, China). Carcinoembryonic antigen (CEA) and α-fetoprotein (AFP) were purchased from Beijing Keybiotech Co. Ltd. (China). Aminoterminal pro-brain natriuretic peptides (NT-proBNP), recombinant SARS-CoV-2 nucleocapsid protein (SARS-CoV-2 NP), anti-SARS-CoV-2 NP antibodies (mouse monoclonal antibodies, clone Nos. 8B1 and 9B3) were obtained from FANTIBODY (Chongqing, China). BCA protein kit was purchased from KeyGEN BioTECH Corp. Ltd (Jiangsu, China). Hemin labeled oligonucleotides were purchased from Takara Bio Inc. (Beijing, China). Other DNA oligonucleotides and Bovine serum albumin (BSA) were obtained from Sangon Biotechnology Co. Ltd. (Shanghai, China). UltraPowerTM DNA dye was purchased from Bio-Teke Biotechnology Co. (Beijing, China). The DNA sequences were listed in Table S1. Ultrapure water from a Millipore water purification system (Milli-Q, Millipore) was used for all experiments.

2.2. Apparatus

CL images were captured by BioSpectrum 615 Imaging System, and analyzed using VisionWorks image acquisition and analysis software (UVP, USA). CL kinetic curves were obtained using MPI-A multifunctional electrochemical and chemiluminescence analytical system with a flow injector (Xi'an Remex Analytical Instrument Co., Ltd. China). Fluorescence decay curve of luminol was collected by FLS980 Photoluminescence Spectrometer (Edinburgh Instruments Ltd., UK). Fluorescence spectra was collected on Hitachi F-7000 fluorescence spectrophotometer (Hitachi, Japan). The gel electrophoresis was

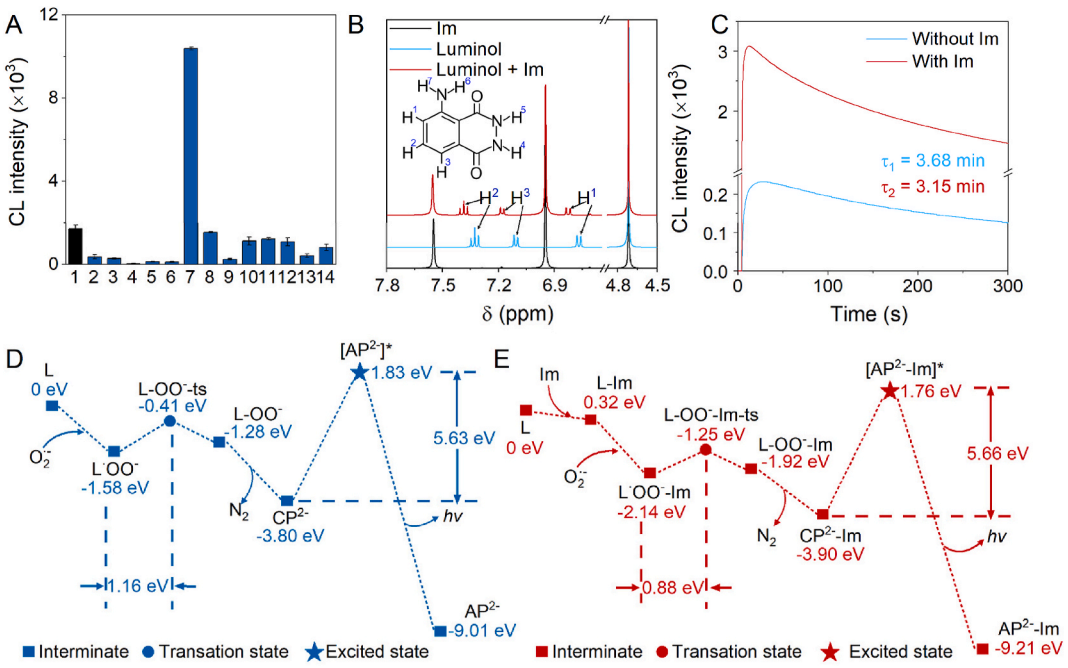

Fig. 1. (A) CL intensity of 10 mM pH 7.2 PBS containing 0.4 mM luminol, 1 mM H_2O_2, and 20 nM hemin-D1 in absence (column 1) and presence of 4 mM *p*-iodophenol, naphthol, 4-chlorothiophenol, 1,4-naphthalenedicarboxylic acid, tryptophan, Im, 2-methylimidazole, imidazole-2-carboxaldehyde, histidine, arginine, polyvinyl pyrrolidone, lysine homopolymer hydrobromide and chitosan (columns 2 to 14). (B) ^{1}H NMR spectra of Im, luminol and the mixture of luminol and Im in DMSO-*d6*. (C) CL kinetic curves of 10 mM pH 7.2 PBS containing 0.4 mM luminol, 1 mM H_2O_2 and 20 nM hemin-D1 in absence and presence of 4 mM Im. DFT calculations of (D) luminol oxidation process and (E) Im-enhanced luminol oxidation process. Error bars: mean ± SD, $n = 3$.

performed on Mini-PROTEAN Tetra System (Bio-RAD, USA) and imaged on BioSpectrum 615 Imaging System.

2.3. Preparation of double strand hemin-DNA hybrid

Double strand hemin-DNA hybrids, hemin-D1/D2-hemin and hemin-D3/D4-hemin, were prepared by mixing hemin-D1 and hemin-D2 (or hemin-D3 and hemin-D4) at 1:1 ratio. After the mixture was annealed at 95 °C for 5 min and cooled to room temperature, the double strand hemin-DNA hybrids hemin-D1/D2-hemin and hemin-D3/D4-hemin were obtained. The obtained products were diluted to 1 μM with PBS (pH 7.2, 10 mM) and stored at 4 °C for further use.

2.4. Preparation of DNM

After separately mixed block-1 with primer-1 and block-2 with primer-2 at a ratio of 1:1, the DNA hybrids C1 and C2 were obtained by annealing the mixtures at 95 °C for 5 min and then cooling to room temperature. Afterword, C1 (10 μL, 10 μM), C2 (10 μL, 10 μM), liner (10 μL, 10 μM) and DNA skeleton (5 μL, 10 μM) were mixed for the assembly of DNM at 37 °C for 30 min. The obtained products of DNM were diluted to 1 μM with PBS (pH 7.2, 10 mM) and stored at 4 °C for further use.

2.5. Preparation of affinity probes

Affinity probes were synthesized using MBS as the linker. Briefly, 20 μL of 2 mg/mL Ab1 (or Ab2) was firstly mixed with 40-fold molar excess of MBS in PBS (pH 7.2, 10 mM) with a total volume of 200 μL, and incubated at room temperature for 2h. Meanwhile, 10 μL of 100 μM P1 (or P2) was mixed with 150-fold molar excess of TCEP in PBS (pH 5.5, 10 mM) with a total volume of 200 μL, and incubated at room temperature for 2h. Afterward, the reaction product Ab1 (or Ab2) with MBS (Ab1-MBS or Ab2-MBS) was purified by ultrafiltration (30 kDa, 8000 rpm, 5min for 8 times), and the reaction product of P1 (or P2) with TCEP was also purified by ultrafiltration (10 kDa, 12000 rpm, 10min for 5 times). The obtained Ab1-MBS (or Ab2-MBS) complex was mixed with reduced P1 (or reduced P2) to incubate for 2 h at room temperature. The obtained affinity probe Ab1-P1 (or Ab2-P2) was purified by ultrafiltration (50 kDa, 8000 rpm, 5min for 8 times). BCA protein assay kit was used to calibrate the concentrations of affinity probes. The obtained affinity probes were stored at −20 °C for further use.

2.6. Calculations

The Gaussian 16 program was used for all calculations (Frisch et al., 2016). The initial model of the reactants, intermediates, and final products in the luminol oxidization was optimized with B3LYP-D3 functional and the 6-311G(d,p) basis set in water (McLean and Chandler, 1980; Lee et al., 1988; Grimme et al., 2010). The polarizable continuum model with SMD-coulomb atomic radii was used to find the most stable geometry of all intermediates and then search for related reactants in the transition state (Miertuš et al., 1981; Tomasi et al., 2005). After the intrinsic reaction coordinate (IRC) analysis, the transition state was followed by the TS method in two directions, which ensured the correlation of transition state to the correct reactants and products. Only the transition state had an imaginary frequency. Frequency analysis and IRC analysis were performed using the same basis set as the optimization.

2.7. Electrophoresis analysis

The loading samples were prepared by mixing 4 μL analyte with 1 μL UltraPowerTM DNA dye and 1 μL 6 × loading buffer for 5-min incubation. 8 % native polyacrylamide gel was used for PAGE analysis. After loading all samples into the gel, the gel electrophoresis was performed at 100 V for 60 min, and the DNA bands were visualized by BioSpectrum 615 Imaging System.

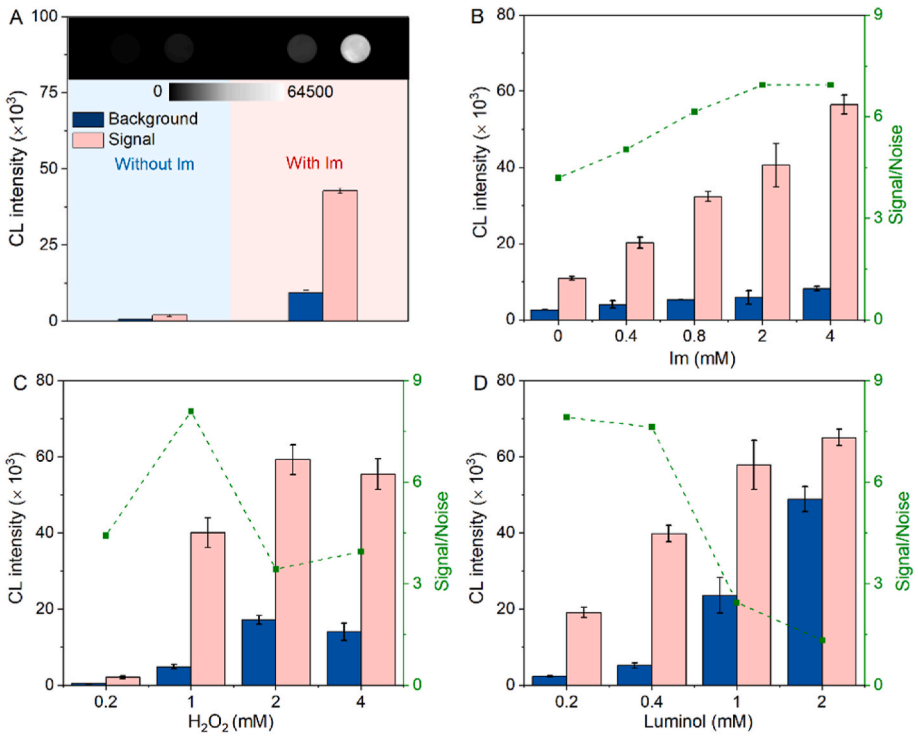

Fig. 2. (A) CL intensity of 10 mM pH 7.2 PBS containing 0.4 mM luminol, 1 mM H_2O_2, 20 nM hemin-D1/D2-hemin without (background) and with (signal) 20 nM primer-1 in the absence (left) and presence (right) of 4 mM Im. (B–D) Effects of Im (B), H_2O_2 (C) and luminol (D) concentration on CL intensity of 10 mM pH 7.2 PBS containing Im (4 mM for C and D), H_2O_2 (1 mM for B and D), luminol (0.4 mM for B and C) and 20 nM hemin-D1/D2-hemin in absence or presence of 20 nM primer-1. Error bars: mean ± SD, $n = 3$.

2.8. CL response to initiator

1 μL initiator at different concentrations were mixed with DNM (2 μL, 1 μM), hemin-D1/D2-hemin (1 μL, 1 μM), hemin-D3/D4-hemin (1 μL, 1 μM) and PBS (5 μL, 10 mM, pH 7.2) to incubate for 20 min at 37 °C. Then 40 uL CL substrate containing 0.5 mM luminol, 5 mM Im and 1.25 mM H_2O_2 was added to perform the CL measurements and collect CL signals with an exposure time of 30 s.

2.9. CL response to SARS-CoV-2 NP

1 μL SARS-CoV-2 NP samples with different concentrations were added into 9 μL solution containing affinity probes (2 μL, 1 μg/mL), iblock/initiator (1 μL, 2 μM), hemin-D1/D2-hemin (1 μL, 1 μM), hemin-D3/D4-hemin (1 μL, 1 μM), DNM (2 μL, 1 μM) and PBS (2 μL, 10 mM, pH 7.2) to incubate for 30 min at 37 °C. Afterward, 40 uL CL substrate containing 0.5 mM luminol, 5 mM Im and 1.25 mM H_2O_2 was added to perform the CL measurements and collect CL images with an exposure time of 30 s.

3. Results and discussion

3.1. Imidazole enhanced hemin-DNA/luminol/H_2O_2 CL system

The hemin-DNA catalyzed luminol/H_2O_2 CL system was firstly evaluated with several commonly used small molecules as the enhancers (Fig. S1) (Liu et al., 2015; Li and Lillehoj, 2021). Only Im exhibited a significant CL enhancement (Fig. 1A), which indicated that Im could be used as an efficient CL enhancer of this system. It was interesting to notice that all negative charged small molecules (column 2 to 6) inhibited the CL signal of luminol/H_2O_2 CL system, but other electropositive molecules also did not enhance the CL performance of luminol/H_2O_2 CL system (column 8 to 14), which implied that the effect of Im to luminol/H_2O_2 CL system was not related to the electrostatic interaction. Im has been proved to be efficient organocatalyst to decrease the reaction energy of the nucleophilic reaction through the formation of two hydrogen bonds (Nguyen et al., 2014), thus the interaction between Im and luminol was evaluated. ^{1}H NMR spectra of luminol showed downfield shift of the peak of H on the benzene ring of luminol in the presence of Im (Fig. 1B), which could be caused by the hydrogen bond-induced reduction of electron density (Min et al., 2012). The FL time-resolved decay curve of luminol showed the increased fluorescence lifetime in the presence of Im (Fig. S2), which indicated the decrease of molecular vibration due to the interaction of Im with luminol through hydrogen bonds (Q. X. Guo et al., 2020; Wang et al., 2025). Furthermore, the CL lifetime of luminol/H_2O_2 system exhibited a slight decrease upon the addition of Im (Fig. 1C), which implied that Im might affect the stability of intermediates in the luminol oxidization process.

In the presence of Im, the HOMO-LUMO gap of luminol (L) was decreased from 2.39 eV to 2.27 eV (Fig. S3), indicating the high reactivity for luminol oxidation (Lai et al., 2019). DFT calculations were performed to demonstrate the Im-assisted luminol oxidation (Fig. 1D and E). After the reactive oxygen species ($O_2^{\bullet-}$) attacked the carboxamide moiety of luminol, an endoperoxide intermediate (L-OO^-) was produced and then experienced the elimination of N_2 to produce unstable dianionic cyclic peroxide (CP^{2-}) intermediate, which quickly generated CL emission by breaking the O-O bond to produce aminophthalate dianion (AP^{2-}) (Giussani et al., 2019) (Fig. S4A). The activation barrier for luminol oxidation with $O_2^{\bullet-}$ was calculated to be 1.16 eV (Fig. 1D). The process of Im-assisted luminol oxidation was shown in Fig. S4B, and the activation barrier for luminol oxidation in the presence of Im was decreased to 0.88 eV (Fig. 1E), revealing that Im could reduce the reaction energy of luminol, which was consistent with the molecular orbital calculations (Fig. S3). Besides, the activation energies to the excited state of AP^{2-} in the absence and presence of Im were calculated to be 5.63 and 5.66 eV, respectively, implying that Im did not impact on the chemical exciting of AP^{2-}. It was worth noting that the total energy

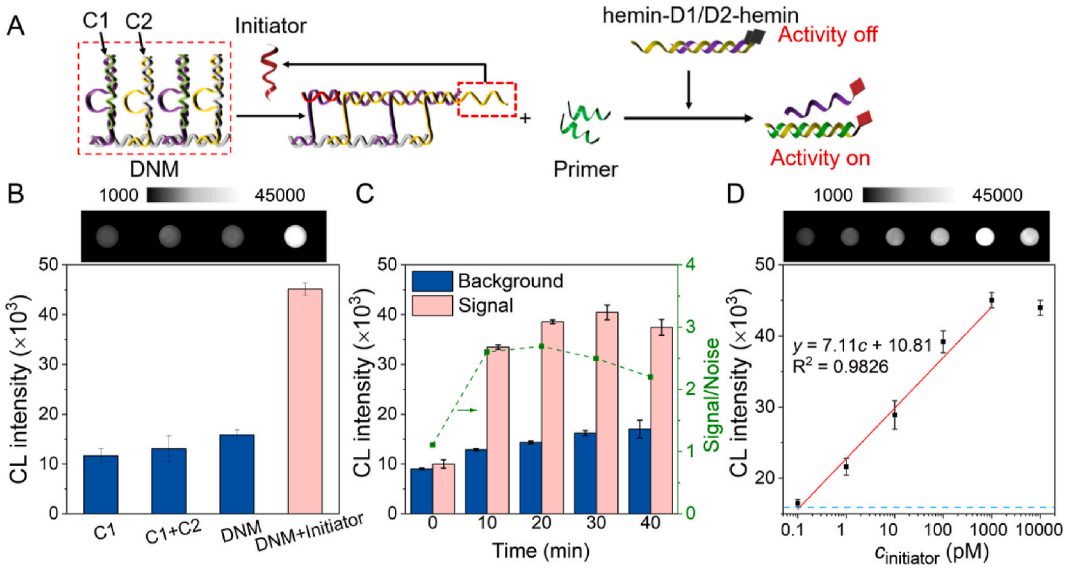

Fig. 3. (A) Structural diagram of initiator-triggered DNM for activating hemin-DNA switch. (B) CL intensity of 10 mM pH 7.2 PBS containing 0.4 mM luminol, 1 mM H_2O_2, 4 mM Im, 20 nM hemin-D1/D2-hemin, 20 nM hemin-D3/D4-hemin and 80 nM C1 or the mixture of 80 nM C1 and C2, or 40 nM DNM, or the mixture of 40 nM DNM and 1 nM initiator. (C) Effect of incubation time on CL signal of initiator-triggered DNM at 1.0 nM initiator. (D) CL intensity of 10 mM pH 7.2 PBS containing 0.4 mM luminol, 1 mM H_2O_2, 4 mM Im, 20 nM hemin-D1/D2-hemin, 20 nM hemin-D3/D4-hemin, 40 nM DNM and initiator at 0.1, 1.0, 10, 100 pM, 1.0 nM and 10 nM and the corresponding calibration curve. Error bars: mean ± SD, $n = 3$.

of CP^{2-} can be convergence in the absence of Im (Fig. S5A), while CP^{2-} could quickly release the energy to produce AP^{2-} in the presence of Im (Fig. S5B), indicating that Im enhanced the CL signal of luminol/H_2O_2 CL system not only through the reduction of the activation barrier for luminol oxidation, but also assisting the breaking of O-O bond to generate CL emission. 1,2,4-Triazole (Tz) exhibited the similar CL enhancement effect for luminol/H_2O_2 CL system, while the benzotriazole (BZTA) had a significant quenching effect on this CL system (Fig. S6).

3.2. Im assisted hemin-DNA enzyme activity switch

The effect of Im on the CL switch which was performed by hemin enzymatic activity regulation was further examined. The hemin-DNA dimer (hemin-D1/D2-hemin) exhibited negligible CL signal, and CL intensity increased in the presence of primer-1 (Fig. 2A, left), which was achieved by simple strand displacement reaction to generate hemin-DNA monomers. However, the CL intensity of the hemin-DNA monomer catalyzed luminol/H_2O_2 CL system was still insufficient for CL imaging. Fortunately, the introduction of Im caused significantly CL enhancement (Fig. 2A, right), which enabled CL imaging detection.

At optimal pH of 7.2 for the hemin-DNA switch (Fig. S7), the concentrations of Im, H_2O_2 and luminol for CL imaging were optimized. The maximum signal-to-noise ratio was observed at 2 mM Im (Fig. 2B), while the optimal concentrations of H_2O_2 and luminol were chosen to be 1 mM and 0.4 mM (Fig. 2C and D).

3.3. CL performance of DNM-based signal amplification

The DNM-based signal amplification strategy was designed for activating the hemin-DNA switch (Ren et al., 2018; Zhang et al., 2020). The DNM was composed by C1 (primer1/block1) and C2 (primer2/block2) with a DNA skeleton (Fig. 3A), which provided a high local concentration environment for C1 and C2. Upon the addition of the initiator, the bulge loop of C1 was opened through the hybridization of initiator with block1, and the primer1 was released due to the unstable hybridization between the terminal sequences on the C1 (Fig. S8). The exposed terminal sequence of block1 could hybridized with block2 to open the bulge loop of C2, which released primer2 to expose the terminal sequence of block2. The terminal sequence of block2 contained the same sequence with initiator, thus could triggered the cascade hybridization chain reaction in the DNA skeleton to release another primer1 and primer2 from C1 and C2 to release numerous primers, which turned on the hemin-DNA switch for catalyzing the CL emission reaction.

C1 could not separate the hemin-D1/D2-hemin dimer to generate CL signal, and the mixture of C1 and C2 also caused negligible change in CL signal (Fig. 3B). When DNM was mixed with hemin-D1/D2-hemin dimer, a slight increase of CL intensity was observed, which might be caused by the unavoidable DNA leakage. However, after the addition of a small amount of initiator into the DNM and hemin-D1/D2-hemin contained reaction solution, a significant CL signal could be obtained, indicating the successful construction of DNM-activated hemin-DNA switch. The initiator-induced cascade hybridization reaction was confirmed by PAGE analysis (Fig. S9). The bands of hemin-D1/D2-hemin dimer, hemin-D3/D4-hemin dimer, C1 and C2 did not change when they were mixed (lane 6). However, after the initiator was introduced into the mixture, obvious DNA assembly products with high molecule weight were observed (lane 7), implying the successful signal amplification based on the initiator triggered DNM.

The CL signal of DNM-activated hemin-DNA switch exhibited the time-dependent increase after the addition of initiator, and the signal-to-noise ratio reached the maximum at 20 min, which was use as the incubation time for DNM (Fig. 3C). With the increasing concentration of initiator, the CL signal increased, and the plot of the CL intensity versus the logarithm of the concentration of initiator showed good linearity from 0.1 pM to 1 nM (Fig. 3D), which guaranteed the feasibility of quantitative analysis for SARS-CoV-2 NP detection through DNM-activated hemin-DNA switch combined with proximity binding-induced initiator release.

3.4. CL imaging assay of SARS-CoV-2 NP

The proximity binding-induced initiator release was verified by fluorescence (FL) method. The hybridization of T-DNA with P1 and P2 was used to simulate the recognition of target protein by a pair of affinity probes. After the hybridization of T-DNA with P1 and P2, the formed proximity-ligated oligonucleotide sequence could hybridize with the iblock' from iblock'/initiator' and release initiator' (Fig. S10A). The FL

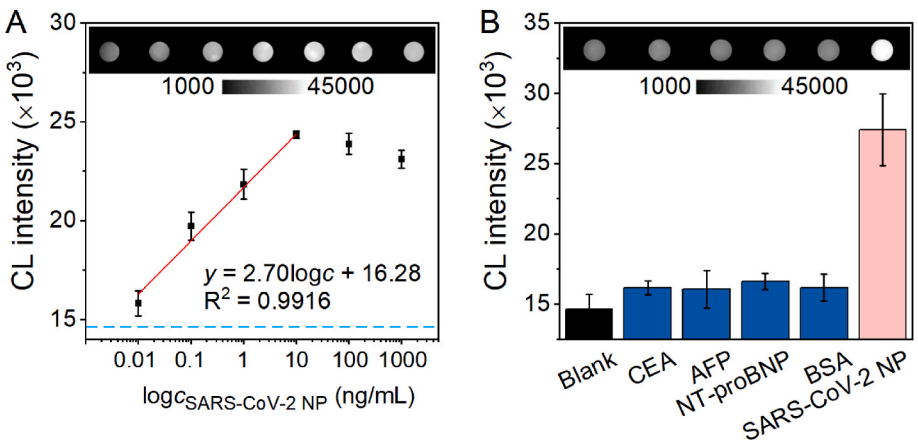

Fig. 4. (A) Calibration curve for SARS-CoV-2 NP CL imaging detection. (B) CL intensity of 10 mM pH 7.2 PBS containing 0.4 mM luminol, 1 mM H_2O_2, 4 mM Im, 20 nM hemin-D1/D2-hemin, 20 nM hemin-D3/D4-hemin, 40 nM DNM, 20 nM iblock/initiator, 20 ng/mL Ab1-P1 and 20 ng/mL Ab2-P2 in the presence of 1 ng/mL CEA, AFP, NT-proBNP, BSA or SARS-CoV-2 NP. Error bars: mean ± SD, $n = 3$.

signal sharply decreased when initiator' was hybridized with iblock' due to the approach of FAM to BHQ (Fig. S10B). The P1, P2 and the mixture of P1 and P2 could not recover the FL signal. However, after the addition of T-DNA, the FL signal was significantly recovered, which proved the successful proximity binding-induced initiator release.

The CL imaging assay of SARS-CoV-2 NP was executive through a pair of affinity probes, which could specifically recognize the SARS-CoV-2 NP at the same time to form a new sequence, then the new sequence could hybridized with the iblock and released the initiator from iblock/initiator for triggering the DNM to open the hemin-DNA switches. The affinity probes Ab1-P1 and Ab2-P2 was obtained by covalently binding of antibodies to probe DNA via MBS linker, which was confirmed by PAGE analysis (Fig. S11). The CL signal reached the maximum value under 20 min incubation (Fig. S12), which was selected as the optimal assay time for SARS-CoV-2 NP. The CL intensity increased with the increasing concentration of SARS-CoV-2 NP, which showed a good linear relationship with the logarithm of SARS-CoV-2 NP concentration ranging from 0.01 to 10 ng/mL (Fig. 4A). A Hook effect can be observed when the concentration of SARS-CoV-2 NP was higher than 10 ng/mL, which was commonly observed in homogeneous immunoassays. The detection limit of the proposed CL imaging assay was calculated to be 2.75 pg/mL, which was higher than the molecular imprinting composite-based electrochemical assay (51.2 pg/mL) (Drobysh et al., 2024), and much higher than the microfluidic immunosensor-based colorimetric assay (10 ng/mL) (Liu et al., 2021) and electrochemical assay (8.89 ng/mL) (Fukana et al., 2025), tyramide signal amplification-based fluorescence assay (48.9 ng/mL) (Huang et al., 2025) for SARS-CoV-2 NP. The specificity of the proposed CL assay was also verified, and only the sample containing SARS-CoV-2 NP exhibited a distinctive CL signal (Fig. 4B), indicating the good selectivity of the proposed CL imaging assay.

3.5. Sample analysis

Recovery experiments were applied to evaluate the accuracy of the proposed CL assay for SARS-CoV-2 NP. Different concentrations of SARS-CoV-2 NP were spiked in human serum samples, and the recovery rate ranged from 89.18 % to 104.0 % (Table S2), which indicated the acceptable reliability of the proposed CL imaging assay.

4. Conclusion

An Im-enhanced hemin-DNA catalyzed luminol/H_2O_2 CL system has been proposed for highly sensitive immunoassay of protein target through forming the hydrogen bonds between Im and luminol to reduce the luminol oxidation energy barrier and accelerate the breaking of O-O bond of CP^{2-} for producing strong CL emission, which leads to a homogeneous CL imaging assay method for the detection of SARS-CoV-2 NP. Upon the recognition of SARS-CoV-2 NP by a pair of affinity probes, the formed proximity-ligated sequence can trigger the release of initiator, which further activates the hybridization chain reaction on DNM to release numerous primers to separate inactive hemin dimer moiety into active hemin monomer moiety and then generate strong CL signal under the assistance of Im. The proposed signal amplification strategy and CL assay method possesses excellent performance, such as high sensitivity, short analytical time, acceptable reliability and high throughput of CL imaging technique, and the potential application in early diagnosis of SARS-CoV-2 NP disease.

CRediT authorship contribution statement

Hang Ao: Writing – original draft, Methodology, Formal analysis, Data curation, Conceptualization. **Jinshan Xiong:** Software, Formal analysis, Data curation. **Wencheng Xiao:** Formal analysis. **Wenrui Hu:** Formal analysis. **Jie Wu:** Writing – original draft, Methodology, Conceptualization. **Huangxian Ju:** Writing – review & editing, Supervision, Funding acquisition, Conceptualization.

Notes

The authors declare no competing financial interest.

Declaration of competing interest

The authors declare that they have no known competing financial interests or personal relationships influencing the work reported in this work.

Acknowledgements

This project was supported by the National Natural Science Foundation of China (21827812, 21890741), Independent Research Project from State Key Laboratory of Analytical Chemistry for Life Science (5431ZZXM2006) and State Key Laboratory of Analytical Chemistry for Life Science (SKLACLS2517).

Appendix A. Supplementary data

Supplementary data to this article can be found online at https://doi.org/10.1016/j.bios.2025.118002.

Data availability

Data will be made available on request.

References

Alsharabasy, A.M., Pandit, A., Farràs, P., 2021. Adv. Mater. 33, 2003883. https://doi.org/10.1002/adma.202003883.

Anderson, G.P., Liu, J.L., Esparza, T.J., Voelker, B.T., Hofmann, E.R., Goldman, E.R., 2021. Anal. Chem. 93, 7283–7291. https://doi.org/10.1021/acs.analchem.1c00677.

Ao, H., Xiao, W.C., Chen, Y.H., Wu, J., Ju, H.X., 2023. Sensor. Actuat. B-Chem. 383, 133579. https://doi.org/10.1016/j.snb.2023.133579.

Davis, H.E., McCorkell, L., Vogel, J.M., Topol, E.J., 2023. Nat. Rev. Microbiol. 21, 133–146. https://doi.org/10.1038/s41579-022-00846-2.

Diao, B., Wen, K., Zhang, J., Chen, J., Han, C., Chen, Y., Wang, S., Deng, G., Zhou, H., Wu, Y., 2021. Clin. Microbiol. Infect. 27, 289.e1–289.e4. https://doi.org/10.1016/j.cmi.2020.09.057.

Drobysh, M., Ratautaite, V., Brazys, E., Ramanaviciene, A., Ramanavicius, A., 2024. Biosens. Bioelectron. 251, 116043. https://doi.org/10.1016/j.bios.2024.116043.

Ferreira, M.D.P., Yamada-Ogatta, S.F., Tarley, C.R.T., 2023. Biosensors 13, 336. https://doi.org/10.3390/bios13030336.

Frisch, M.J., Trucks, G.W., Schlegel, H.B., Scuseria, G.E., Robb, M.A., Cheeseman, J.R., Scalmani, G., Barone, V., Petersson, G.A., Nakatsuji, H., Li, X., Caricato, M., Marenich, A.V., Bloino, J., Janesko, B.G., Gomperts, R., Mennucci, B., Hratchian, H. P., Ortiz, J.V., Izmaylov, A.F., Sonnenberg, J.L., Williams-Young, D., Ding, F., Lipparini, F., Egidi, F., Goings, J., Peng, B., Petrone, A., Henderson, T., Ranasinghe, D., Zakrzewski, V.G., Gao, J., Rega, N., Zheng, G., Liang, W., Hada, M., Ehara, M., Toyota, K., Fukuda, R., Hasegawa, J., Ishida, M., Nakajima, T., Honda, Y., Kitao, O., Nakai, H., Vreven, T., Throssell, K., Montgomery, J.A., Peralta Jr., J.E., Ogliaro, F., Bearpark, M.J., Heyd, J.J., Brothers, E.N., Kudin, K.N., Staroverov, V.N., Keith, T.A., Kobayashi, R., Normand, J., Raghavachari, K., Rendell, A.P., Burant, J. C., Iyengar, S.S., Tomasi, J., Cossi, M., Millam, J.M., Klene, M., Adamo, C., Cammi, R., Ochterski, J.W., Martin, R.L., Morokuma, K., Farkas, O., Foresman, J.B., Fox, D.J., 2016. Gaussian 16, Revision C.01. Gaussian Inc., Wallingford CT. https://gaussian.com/citation.

Fukana, N., Park, J., Junior, G.J.S., Malsick, L.E., Gallichotte, E.N., Ebel, G.D., Geiss, B.J., Dandy, D.S., Bertotti, M., Nacapricha, D., Baldo, T.A., Henry, C.S., 2025. Biosens. Bioelectron. 271, 117048. https://doi.org/10.1016/j.bios.2024.117048.

Giussani, A., Farahani, P., Martínez-Muñoz, Lundberg, M., Lindh, R., Roca-Sanjuán, D., 2019. Chem. Eur J. 25, 5202–5213. https://doi.org/10.1002/chem.201805918.

Grimme, S., Antony, J., Ehrlich, S., Krieg, H., 2010. J. Chem. Phys. 132, 154104. https://doi.org/10.1063/1.3382344.

Golnak, R., Xiao, J., Atak, K., Khan, M., Suljoti, E., Aziz, E.F., 2015. J. Phys. Chem. B 119, 3058–3062. https://doi.org/10.1021/jp509966q.

Guo, L., Ren, L., Yang, S., Xiao, M., Chang, D., Yang, F., Dela Cruz, C.S., Wang, Y., Wu, C., Xiao, Y., Zhang, L., Han, L., Dang, S., Xu, Y., Yang, Q.W., Xu, S.Y., Zhu, H.D., Xu, Y. C., Jin, Q., Sharma, L., Wang, L.H., Wang, J.W., 2020. Clin. Infect. Dis. 71, 778–785. https://doi.org/10.1093/cid/ciaa310.

Guo, Q.X., Liu, Y.H., Liu, M., Zhang, H., Qian, X.Q., Yang, J.J., Wang, J., Xue, W.Y., Zhao, Q., Xu, X.J., Ma, W., Tang, Z., Li, Y.L., Bo, Z.S., 2020. Adv. Mater. 32, 200164. https://doi.org/10.1002/adma.202003164.

Huang, Z.Y., Du, Z.Y., Li, J., He, J.X., Yang, Y.B., Wang, D., Liang, Y., Yang, Y.S., Peng, R. Z., Tan, W.H., 2025. Anal. Chem. 97, 328–336. https://doi.org/10.1021/acs.analchem.4c04225.

Kilic, T., Weissleder, R., Lee, H., 2020. iScience 23, 101406. https://doi.org/10.1016/j.isci.2020.101406.

Kim, J., Lee, S.K., Lee, J.H., Kim, H.Y., Kim, N.H., Lee, C.H., Lee, C.S., Kim, H.G., Lai, Y. P., Huang, J.M., Tang, D.Y., Chen, X.L., Hou, L., Zhao, S.L., Lin, T.R., 2022. Adv. Mater. Interfac. 9, 2102046. https://doi.org/10.1002/admi.202102046.

Lai, T.Y., Guo, J.D., Fettinger, J.C., Nagase, S., Power, P.P., 2019. Chem. Commun. 55, 405–407. https://doi.org/10.1039/c8cc08488b.

Lee, C., Yang, W., Parr, R.G., 1988. Phys. Rev. B 37, 785–789. https://doi.org/10.1103/PhysRevB.37.785.

Li, J.R., Lillehoj, P.B., 2021. ACS Sens. 6, 1270–1278. https://doi.org/10.1021/acssensors.0c02561.

Li, T., Wang, L., Wang, H., Li, X., Zhang, S., Xu, Y., Wei, W., 2020. Front. Cell. Infect. Microbiol. 10, 470. https://doi.org/10.3389/fcimb.2020.00470.

Liu, D., Ju, C.H., Han, C., Shi, R., Chen, X.H., Duan, D.M., Yan, J.H., Yan, X.Y., 2021. Biosens. Bioelectron. 173, 112817. https://doi.org/10.1016/j.bios.2020.112817.

Liu, L., Zhang, L.L., Fu, C.Y., Wang, Y.S., Sun, S.H., 2015. Luminescence 30, 1297–1302.

Lyu, A.H., Jin, T.C., Wang, S.S., Huang, X.X., Zeng, W.H., Yang, R., Cui, H., 2021. Sensor. Actuat. B-Chem. 349, 130739. https://doi.org/10.1016/j.snb.2021.130739.

McLean, A.D., Chandler, G.S.J., 1980. Chem. Phys. 72, 5639–5648. https://doi.org/10.1063/1.438980.

Miertuš, S., Scrocco, E., Tomasi, J., 1981. Chem. Phys. 55, 117–129. https://doi.org/10.1016/0301-0104(81)85090-2.

Min, T., Fettinger, J.C., Franz, A.K., 2012. ACS Catal. 2, 1661–1666. https://doi.org/10.1021/cs300290j.

Nguyen, T.B., Ermolenko, L., Dau, M.E.T.H., Al-Mourabit, A., 2014. Heterocycles 88, 403–416. https://doi.org/10.3987/com-13-s(s)41.

Ogata, A.F., Maley, A.M., Wu, C., Gilboa, T., Norman, M., Lazarovits, R., Mao, C.P., Newton, G., Chang, M., Nguyen, K., Kamkaew, M., Zhu, Q., Gibson, T.E., Ryan, E.T., Charles, R.C., Marasco, W.A., Walt, D.R., 2020. Clin. Chem. 66, 1562–1572. https://doi.org/10.1093/clinchem/hvaa213.

Perveen, S., Negi, A., Gopalakrishnan, V., Panda, S., Sharma, V., Sharma, R., 2023. Clin. Chim. Acta 538, 139–156. https://doi.org/10.1016/j.cca.2022.11.017.

Rani, A.Q., Zhu, B., Ueda, H., Kitaguchi, T., 2023. Analyst 148, 1422–1429. https://doi.org/10.1039/D2AN01913B.

Ren, K.W., Zhang, Y., Zhang, X.B., Liu, Y., Yang, M., Ju, H.X., 2018. ACS Nano 12, 10797–10806. https://doi.org/10.1021/acsnano.8b02403.

Shan, D., Johnson, J.M., Fernandes, S.C., Suib, H., Hwang, S.M., Wuelfing, D., Mendes, M., Holdridge, M., Burke, E.M., Beauregard, K., Zhang, Y., Cleary, M., Xu, S., Yao, X., Patel, P.P., Plavina, T., Wilson, D.H., Chang, L., Kaiser, K.M., Nattermann, J., Schmidt, S.V., Latz, E., Hrusovsky, K., Mattoon, D., Ball, A.J., 2021. Nat. Commun. 12, 1931. https://doi.org/10.1038/s41467-021-22072-9.

Shi, F., Peng, M.Y., Zhu, H.B., Li, H.B., Li, J., Hu, X.Y., Zeng, J.B., Yang, Z.J., 2023. Anal. Chem. 95, 14516–14520. https://doi.org/10.1021/acs.analchem.3c03702.

Shi, F., Zhu, H.B., Li, G.L., Peng, M.Y., Cao, Y., Xia, Y.P., Ren, C.L., Li, J., Yang, Z.J., 2025. Anal. Chem. 97, 7128–7137. https://doi.org/10.1021/acs.analchem.4c06387.

Sun, Y., Xie, Z.H., Pei, F.B., Hu, W., Feng, S.S., Hao, Q.L., Liu, B., Mu, X.H., Lei, W., Tong, Z.Y., 2022. Anal. Methods 14, 5091–5099. https://doi.org/10.1039/d2ay01530g.

Takkinen, K., Žvirblienė, A., 2019. Curr. Opin. Biotechnol. 55, 16–22. https://doi.org/10.1016/j.copbio.2018.07.003.

Tomasi, J., Mennucci, B., Cammi, R., 2005. Chem. Rev. 105, 2999–3093. https://doi.org/10.1021/cr9904009.

Wang, D., Zhang, J., Huang, Z., Yang, Y., Fu, T., Yang, Y., Lyu, Y., Jiang, J., Qiu, L., Cao, Z., Zhang, X., You, Q., Lin, Y., Zhao, Z., Tan, W., 2023. ACS Cent. Sci. 9, 72–83. https://doi.org/10.1021/cr9904009.

Wang, Q.B., Xu, N., Gui, Z., Lei, J.P., Ju, H.X., Yan, F., 2014. Chem. Commun. 50, 15362–15365. https://doi.org/10.1039/c4cc07298g.

Wang, Q.B., Xu, N., Gui, Z., Lei, J.P., Ju, H.X., Yan, F., 2015. Analyst 140, 6532–6537. https://doi.org/10.1039/c5an01206f.

Wang, Y.Y., Xiong, Z.P., Wang, Y.N., Li, A.S., Fang, Y.Y., Li, L., Wang, K., Li, Q., Zhang, H. K., 2025. Angew. Chem. Int. Ed. 64, e202420502. https://doi.org/10.1002/anie.202420502.

Xiao, Q., Xu, C.X., 2020. Trends Anal. Chem. 124, 115780. https://doi.org/10.1016/j.trac.2019.115780.

Xu, Y., Xia, C., Zeng, X., Qiu, Y.L., Liao, M.J., Jiang, Q., Quan, M.F., Liu, R.S., 2022. J. Virol. Methods 302, 114486. https://doi.org/10.1016/j.jviromet.2022.114486.

Zhang, R., Wu, J., Ao, H., Fu, J.L., Qiao, B., Wu, Q., Ju, H.X., 2021. Anal. Chem. 93, 9933–9938. https://doi.org/10.1021/acs.analchem.1c02229.

Zhang, Y., Chen, W.W., Zhang, Y., Zhang, X.B., Liu, Y., Ju, H.X., 2020. Angew. Chem. Int. Ed. 59, 21454–21459. https://doi.org/10.1002/anie.202009263.